

Contents

2	1	Experimental results	2
3		<i>Diamond irradiation study</i>	
4	1.1	Measurement setup	3
5	1.1.1	Preamplifiers	3
6	1.1.2	Diamond samples	5
7	1.1.3	Readout devices	6
8	1.1.4	Setup for the efficiency study using β particles	6
9	1.1.5	α -TCT setup	7
10	1.1.6	Cryogenic α -TCT setup	7
11	1.2	Particle and photon pulses and spectra	9
12	1.2.1	Noise limitations	9
13	1.3	Radiation limitations	10
14	1.3.1	Quantifying radiation damage in diamonds	11
15	1.3.2	Long-term measurement stability	14
16	1.4	Temperature limitations	20
17	1.4.1	Temperature-variant α -TCT before irradiation	20
18	1.4.2	Temperature-variant α -TCT after irradiation	21
19	1.5	Conclusion	27

²⁰ **Chapter 1**

²¹ **Experimental results**

²² *Diamond irradiation study*

²³ This chapter contains the measurement results of data taken with diamond sensors.
²⁴ First the measurement setup is described (section 1.1). Then the measured particle
²⁵ spectra are shown in 1.2. This is followed by a study of effects of irradiation damage
²⁶ on the electrical signal of the diamond detector and its lifetime. The last section
²⁷ shows the results of the measurements of irradiated diamond samples at cryogenic
²⁸ temperatures. The aim of these studies is to find the operational limitations of dia-
²⁹ mond detectors for spectroscopy and tracking applications. The studies compare the
³⁰ experimentally acquired data with the theory from the previous chapter and define
³¹ limitations of the diamond detectors in terms of noise, radiation and temperature.

³² Diamond sensors are mainly used for two types of measurements: particle counting
³³ and spectroscopy. The first type of measurements depends on the sensor's efficiency –
³⁴ the ability to detect all or at least a known percentage of radiation quanta (particles
³⁵ or photons) that hit it. The energy of the radiation is not so important; what bears
³⁶ the information is the rate and the spatial distribution. Here the radiation does
³⁷ not necessarily stop in the bulk, but rather continues its way. In spectroscopy, on
³⁸ the other hand, the idea is that a particle stops within the sensor, depositing all
³⁹ its energy, which is then measured via the freed charge carriers. The aim of the
⁴⁰ experiments described in this chapter is to:

- ⁴¹ 1. Quantify the efficiency of the sCVD diamond in counting mode,
- ⁴² 2. Quantify the degradation of efficiency with respect to the received radiation
dose,
- ⁴⁴ 3. Quantify the macroscopic effects on charge carrier behaviour with respect to
the received radiation dose and
- ⁴⁶ 4. Define limitations for its use in spectroscopy.

⁴⁷ The results discussed here show that there are several limitations for using diamond as
⁴⁸ a measurement device. All of them need to be taken into account for the measurement

CHAPTER 1. EXPERIMENTAL RESULTS
DIAMOND IRRADIATION STUDY

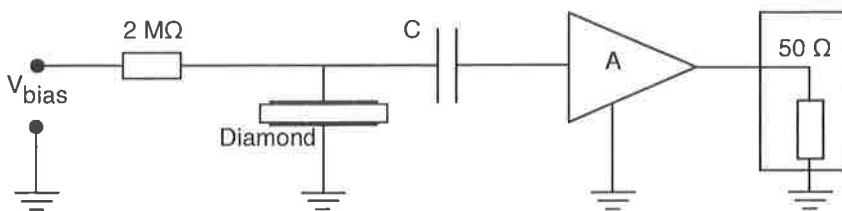


Figure 1.1: Diagram of a diamond detector readout chain.

device to perform reliably and stably. The first step is to build a setup that is insensitive to environmental interferences and minimises electrical noise in the system. The setup needs to be calibrated before use. Then, the measurement conditions have to be defined, such as the temperature, the type of radiation and its flux. This allows us to estimate the lifetime of the detector and predict the longterm change of the signal. This change can then be accounted for when interpreting the output data.

1.1 Measurement setup

To get reliable measurement results, great care has to go towards designing a measurement setup that minimises the noise in the measurements. Shielding has to be applied wherever possible. For instance, aluminium foil can be wrapped around the exposed parts of the system to shield them from external radio-frequency (RF) interferences. In addition, the sensors have to be covered to prevent the light from shining directly onto them.

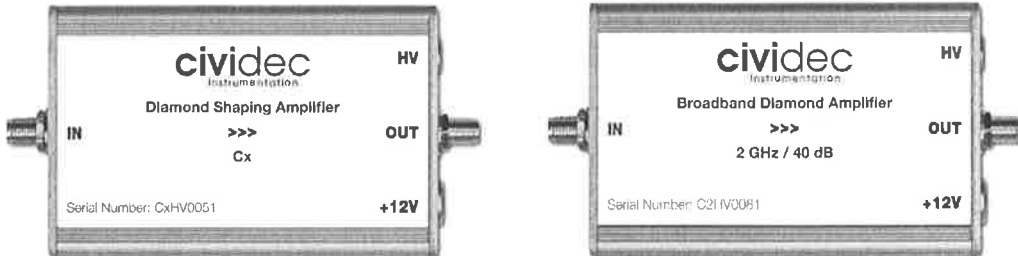
The measurements using diamond that are explained in these chapters were carried out using several measurement setups, but they are all similar in terms of the electrical signal chain. The measurement chain consists of three main parts: a diamond sensor, a signal preamplifier and a readout device, as seen in diagram 1.1. The signals propagating along the analogue chain (before being digitised by the readout device) are fast – in the GHz bandwidth range – and with low amplitudes, which gives rise to importance of RF shielding. Also, the connection between the carrier and the preamplifier has to be as short as possible to avoid capacitive signal losses in the transmission line. Finally, the system needs to be grounded properly.

1.1.1 Preamplifiers

Two preamplifiers were used for the measurements, one sensitive to charge and the other to current. *CIVIDEC Cx* (figure 1.2a) is a charge shaping amplifier. Its high SNR (low noise of 400 electrons) and a reported gain of $\sim 8.2 \text{ mV/fC}$ makes it a good choice for spectroscopic measurements with diamond sensors. *CIVIDEC C2* (figure 1.2b) is a fast current preamplifier with a 2 GHz bandwidth limit. It is used for TCT measurements because of its fast response and a good SNR. Both are

① define noise as $\frac{ENC}{\sqrt{3}} = 400 \text{ e}^-$
(noise in rms of V/I fluctuations!)

1.1. MEASUREMENT SETUP



(a) Cx charge shaping preamplifier

(b) C2 fast charge preamplifier

Figure 1.2: Amplifiers used for the charge and current measurements

78 embedded in an RF-tight aluminium box to reduce the noise pickup. Both have an
79 AC coupled input and an output with a $50\ \Omega$ termination.

80 Calibration

81 The amplifiers were calibrated before use to determine their gain. Both were cali-
82 brated using a square signal generator with a known amplitude step of $U_{in} = (252 \pm$
83 $5)$ mV. A 2 GHz oscilloscope with a 10 GS/s sampling was used to carry out these
84 measurements.

85 In the case of the Cx charge sensitive amplifier, the signal was routed through a
86 capacitor with a calibration capacitance $C_{cal} = (0.717 \pm 0.014)$ pF and then to the
87 input of the amplifier. The pulse area behind the capacitor was $a_{cal} = 5.0 \pm 0.5$ pVs
88 and the signal amplitude on the output was $U_{amp} = (1.95 \pm 0.05)$ V. The input
89 voltage step combined with the calibration capacitance yields a calibration charge
90 $Q_{cal} = C_{cal} \cdot U_{in} = (181 \pm 5)$ fC. The gain of the Cx amplifier is therefore $A_{Cx}^Q = \frac{U_{amp}}{Q_{cal}} =$
91 (9.3 ± 0.4) mV/fC or $A_{Cx}^a = \frac{U_{amp}}{a_{cal}} = (390 \pm 40)$ mV/pVs. The area-based amplification
92 factor has a higher uncertainty ($\sim 10\%$) than the amplitude-based factor ($\sim 4\%$)
93 due to the measurement limitations of the oscilloscope. Nevertheless, it can be used
94 as an estimate for the integrated charge of a current pulse.

$$\begin{aligned} & \leftarrow \\ & \text{is } U_{Cx} \\ & = \\ & V_{amp}^2 \end{aligned}$$

95 To calibrate the C2 current amplifier, only the amplitude gain had to be measured.
96 The input signal amplitude had to be such that it kept the output amplitude within
97 the amplifier's linear range, that is ± 1 V. The signal from the generator was therefore
98 routed through a 36 dB attenuator to decrease its amplitude to $U_{inAtt} = (3.95 \pm$
99 $0.05)$ mV. Two amplifiers with different gains were measured, because both were
100 used for the measurements at different times. The output of the first amplifier was
101 $U_{C2-1} = (860 \pm 5)$ mV. This yields the amplification gain equal to $A_{C2-1} = \frac{U_{inAtt}}{U_{C2-1}} =$
102 (217 ± 3) . The second amplifier had the output equal to $U_{C2-2} = (632 \pm 5)$ mV with
103 the gain equal to $A_{C2-2} = (152 \pm 3)$.

CHAPTER 1. EXPERIMENTAL RESULTS

DIAMOND IRRADIATION STUDY

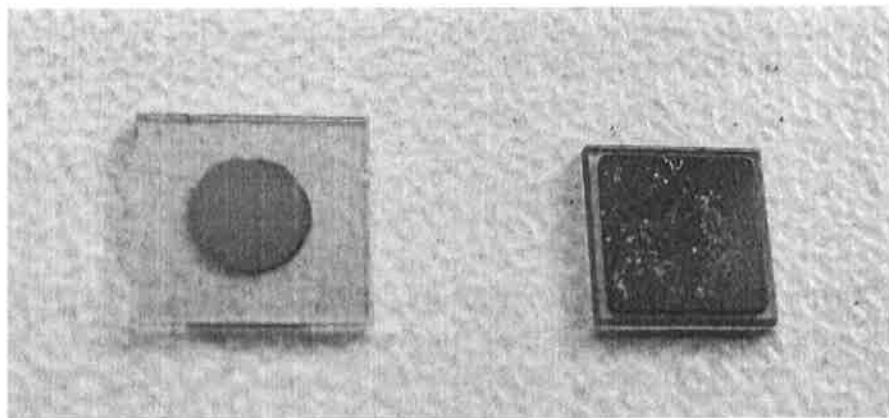


Figure 1.3: Two scCVD diamond samples: A IIa 1scdhq (left) and an E6 S37 (right)

104 1.1.2 Diamond samples

105 Detector-grade diamonds are very difficult to produce, mostly because it is very dif-
106 ficult to ensure a high enough purity of the lattice. It takes companies years of trials
107 to produce high-enough-quality product. Since the target market are almost exclu-
108 sively particle physics research institutes, the companies work closely with them to
109 make sure the product is up to par with the requirements. All sensor samples used
110 to carry out these studies were bought at Element Six (E6). They all have the same
111 standard dimensions. sCVD diamonds with dimensions $4.7 \times 4.7 \text{ mm}^2$ are already
112 sufficiently large for most of the beam monitoring applications and still affordable; the
113 cost of sCVD diamonds grows exponentially with the area. There is also an ongoing
114 race among the producers to produce larger and larger diamonds while maintaining
115 the same cost. For instance, a new company IIa [] from Singapore has produced
116 high-quality samples with larger dimensions and the diamond detector community
117 is currently involved in extensive tests of their products. One of the samples with
118 dimensions of $5.6 \times 5.3 \text{ mm}^2$ was also sent to CERN to be characterised. The target
119 thickness for all the samples is $500 \mu\text{m}$. Diamonds this thick yield a high enough
120 signal-to-noise ratio for MIPs to be measured by the electronics. Table 1.1 shows all
121 the samples used for this study. Two of them were later irradiated with 300 MeV
122 pions and then compared to the pre-irradiated state. Irradiation doses for damaging
123 the material need to be high – above 10^{12} particles per cm^2 to be able to observe
124 change in the sensor's behaviour.

125 Name	Type	Producer	Dimensions (x, y) [mm ²]	Thickness [μm]	Irradiated
S37	sCVD	E6	4.7×4.7	548	no
S50	sCVD	E6	4.7×4.7	537	no
S52	sCVD	E6	4.7×4.7	515	$1 \times 10^{14} \pi_{300 \text{ MeV}} \text{ cm}^{-2}$
S79	sCVD	E6	4.7×4.7	529	$3.63 \times 10^{14} \pi_{300 \text{ MeV}} \text{ cm}^{-2}$
ELSC	sCVD	E6	4.7×4.7	491	no
1scdhq	sCVD	IIa	5.6×5.3	460	no

127 Table 1.1: Diamond sensor samples used

/ include electrode info
in table

② produced by IIa Singapore,

1.1. MEASUREMENT SETUP

E6

The diamond samples have quoted impurity densities of $\leq 2 \times 10^{14} \text{ cm}^{-3}$ and nitrogen incorporation of $\leq 1 \text{ ppb}$. The electrodes were added by various companies and institutes. For instance, S52 was metallised by a company DDL [] while the Physics Department of the University of Firenze, Italy metallised the S79. There are also several techniques for producing the electrodes. The DDL contacts consist of three layers: DLC (diamond-like carbon)/Pt/Au with 4/10/200 nm thicknesses, respectively. The metallisation for S79, on the other hand is made up of Cr/Au with a total thickness of $\sim 400 \text{ nm}$. The area coverage also differs from sample to sample. Diamonds must not be metallised until the very edge as the proximity of contacts with a high potential can lead to sparking. However, since only the areas ~~not~~ covered by the metallisation are sensitive, this effectively reduces the sensitive area of the sensors. In the diamonds used here the effective area was anywhere from 9 mm^2 to 18 mm^2 . Leakage current through the bulk was below 1 ns, but increased for the irradiated samples. The capacitance was of the order of $(2.0 \pm 0.3) \text{ pF}$.

not strictly true
a -

1.1.3 Readout devices

Electrical signals in diamond detectors are in the GHz frequency range. To preserve this information, the readout device has to have a high bandwidth limit. For instance, a 250 MHz limit is enough for the spectroscopic measurements with the Cx charge amplifier, but might be insufficient for the current measurements with the C2 amplifier. Two devices were used take data shown in this chapter. The first choice was a 2 GHz LeCroy WaveRunner 204MXi-A. This specific model has a high enough limit for the fast current preamplifier signals. It offers a versatile solution for analogue signal readout – it is fast to set up and reliable. It is very convenient for use in lab tests and for experiments where small amounts of data are taken and where speed is not crucial. However, its slow acquisition speed turned out to be a bottleneck in the test beam experiment. Its initial 100 Hz readout rate decreased to a mere 20 Hz within 20 minutes, because every single trigger was saved as a separate file and the Windows operating system was not capable of handling 10000+ files in a single directory easily. This is why it was exchanged with a DRS4, an analogue readout device developed by PSI, Switzerland. This compact device is capable of recording up to four waveforms at a time at a steady rate of up to 500 Hz. Its 700 MHz bandwidth limitation was sufficient for the signal from the charge amplifier.

→ add ref.

1.1.4 Setup for the efficiency study using β particles

The efficiency study of the diamond sensors was carried out at CERN in the North Hall test beam facility. There a straight high-energy particle beam of $\pi_{120} \text{ GeV}$ was provided to the users to calibrate their detectors. The beam had a transverse spread of $\sigma = 10 \text{ mm}$ in both axes. The particle rate was of the order of $10^4 \pi \text{ cm}^{-2} \text{ s}^{-1}$. A diamond sensor embedded in a PCB carrier was placed in the beam spot perpendicular to the beam. It was connected via an SMA connector directly to a charge amplifier (described below). The amplified signal was read out using a LeCroy oscilloscope and

CHAPTER 1. EXPERIMENTAL RESULTS

DIAMOND IRRADIATION STUDY

168 a DRS4 analogue readout system (both described below). A computer was used as
169 a controller and data storage for the readout device. A separate ~~system~~ was used as
170 a reference detector. It is called the *beam telescope* and is a device used to cross-
171 check the measurements of the devices under test (DUTs) and to carry out spatially
172 resolved studies on the DUTs. It consists of several pixellated sensor planes placed
173 in series, which can track a particle's trajectory with a precision of a few ~~microns~~ ^{Mm}
174 The sensor planes are positioned in front of the DUT and behind it. Then the beam
175 telescope acts as a trigger system – it triggers the readout of both the telescope data
176 and DUT data when both the planes in front and behind the DUT recorded a hit by
177 the ~~impinging~~ ³ particle. A particle detected by all the planes within the DUT window
178 and the DUT itself counts towards its efficiency whereas a hit missed by the DUT
179 counts against it. To discard the hits missing the DUT, a region of interest (ROI)
180 can be chosen in the beam telescope planes.

181 1.1.5 α -TCT setup

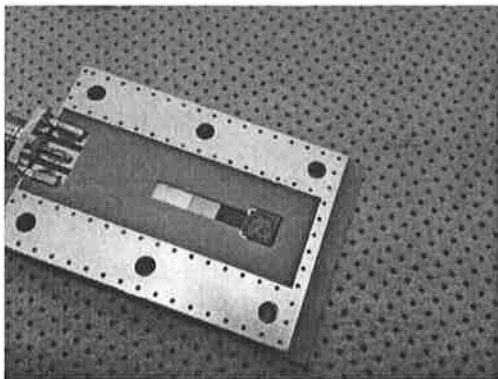
182 Room-temperature TCT measurements were carried out in the lab. The setup con-
183 sisted of a diamond sensor embedded in a PCB carrier, a current amplifier and an
184 oscilloscope. To measure α particles, their energy loss during their trajectory had
185 to be minimised. Therefore the diamond was placed inside a vacuum chamber. The
186 chamber was a steel tube with a diameter of 5 cm. On one side it was connected to a
187 vacuum pump via a steel pipe. A feedthrough with an SMA connector was placed on
188 the other side. A C2 current amplifier was connected directly onto the feedthrough.
189 The amplified output was connected to the oscilloscope via an SMA cable. An ²⁴¹Am
190 source with a diameter of 2 cm and a height of 0.5 cm was fixed onto the sensor carrier
191 (figure 1.4a, figure 1.4b). Then the carrier was inserted in the chamber and fixed in
192 place using an air-tight clamp. The pump was then switched on. It was capable of
193 providing the inside pressure as low as 10^{-4} mbar after approximately one hour of op-
194 eration, but measurements could take place even after five minutes of evacuation, at
195 around 10^{-3} mbar. The most important thing to bear in mind was to switch the bias
196 voltage of the sensor OFF during the process of evacuation, because the air becomes
197 more conductive at the pressure of the order of 10^{-1} mbar []. A failure to switch off
198 the bias voltage would cause a spark between the signal and ground line, destroying
199 the amplifier. ~~and that this can measure~~
^{from RT to ~60K}

200 1.1.6 Cryogenic α -TCT setup

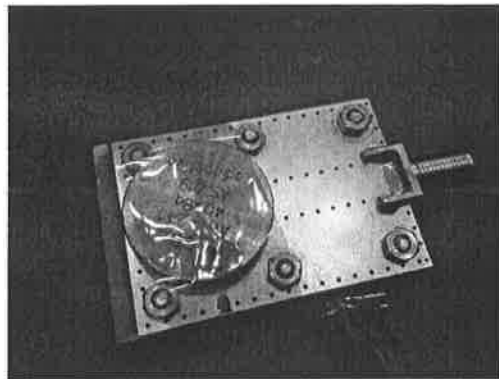
201 The experiment at cryogenic temperatures was carried out in the cryolab at CERN.
202 The room-temperature TCT setup had to be modified to allow for measurements at
203 temperatures as low as 2 K. It consisted of three parts: 1) a cryostat – a thermally
204 insulated cylinder capable of containing liquid helium, 2) an inlet – an air-tight me-
205 chanical tube with valves and feedthroughs at the top that is lowered in the liquid
206 helium and 3) the diamond sample, a temperature sensor, a heater and cables leading
207 to the feedthroughs. The setup is described in detail in [].

³ Define efficiency as: $\epsilon = \frac{N_{\text{DUT}} \wedge N_{\text{Telescope}}}{\text{with acceptance area of DUT} \quad N_{\text{Telescope}}}$

1.1. MEASUREMENT SETUP



(a) PCB carrier with an embedded diamond sample



(b) Radioactive source over the carrier sample

Figure 1.4: Positioning of the α -source on top of the sensor carrier

When the diamond sample was placed in the PCB carrier and the ^{241}Am source was in place, the inlet was sealed and lowered in the empty cryostat. Then the inside volume of the inlet was evacuated to down to 10^{-5} mbar while the liquid helium was flowing into the cryostat. To improve the thermal contact between the diamond and the outside of the inlet, a small amount of helium gas was added inside the evacuated inlet, setting the vacuum to around 10^{-3} mbar. This value changed with time, because the gas condensed on the walls of the inlet, reducing the number of floating particles. For this reason the helium gas had to be added on an irregular basis. Every addition caused a significant undershoot of the sample temperature, which had to be corrected for with a heater placed on the back of the PCB carrier. Also, the added gas deteriorated the vacuum inside the inlet. It was very important to monitor the pressure so as not to let it rise above 10^{-2} mbar. The air at this pressure is significantly more conductive and could cause a short circuit between the two diamond plates or in the SMA connectors, destroying the amplifier. Furthermore, at approximately 60 K the helium gas had to be evacuated from the inlet to avoid a potential explosion due to the expansion of the gas with temperature.

When the sample was cooled to the minimum temperature achievable by use of liquid helium without over-pressurising it (4.2 K), the measurements started. After every temperature data point, the current through the heater placed in the PCB next to the diamond sample was increased, warming up the sample. The initial temperature time constant of the order of tenths of seconds at low temperatures increased with temperature and even more so when helium was evacuated from the inlet at 60 K, removing the thermal bridge between the wall of the inlet and the diamond sample. At the room temperature (RT), the time constant increased to the order of minutes.

How was the temperature of
the sample measured?

(5) very which sources because signal
 $\alpha = ?$ $\gamma = ?$ is energy dependent
 $\beta = ?$

CHAPTER 1. EXPERIMENTAL RESULTS DIAMOND IRRADIATION STUDY

Charged Photons are also particles

1.2 Particle and photon pulses and spectra

In previous chapter the ionisation profiles for different types of radiation were discussed. It is known that β and γ radiation induces a triangular electric pulse whereas α radiation induces a rectangular one. However, their amplitude, width and rise/fall time depend heavily on the type of interaction with the diamond, the purity of the diamond and the bandwidth of the amplifier and the oscilloscope. This section shows the signal pulses of α , β and γ radiation with their respective energy distributions for the case of a diamond detector. Then follows a discussion of effects of noise on these measurements.

A CIVIDEC C2 current amplifier together with the LeCroy oscilloscope (both with a bandwidth limit of 2 GHz) was used to record the pulse shapes whereas the Cx charge amplifier was used for ~~area distribution~~ measurement. A 2 GHz bandwidth limit defines the minimum rising time equal to $t_r \simeq \frac{0.34}{BW} = \frac{0.34}{2 \times 10^9} = 170$ ps, therefore the system is capable of measuring pulses with a minimum FWHM $\simeq 170$ ps. This already makes it impossible to measure the initial peak in the α response due to the two flavours of charge carriers travelling. If a charge carrier travelling through the bulk takes $t_{t1} \sim 6$ ns to get to the electrode on the other side ($d_1 \sim 500$ μm), the carrier with the opposite charge and a shorter path to the closer electrode – max. $d_2 \sim 10$ μm – already ~~recombines~~ in $t_{t2} \sim \frac{d_2}{d_1} t_{t1} = 120$ ps. This is too fast for the C2 amplifier or the oscilloscope to be able to observe.

Figure 1.5 shows a set of pulses and an averaged pulse for α , β and γ radiation as measured by the non-irradiated sCVD diamond S37. α particles always produce the same signal pulse, but with a high noise RMS. The averaging suppresses the noise while still retaining most of the information. It does, however, smear the rising and falling edge, increasing the rise time. The t_r is now of the order of 0.5 ns. Both β and γ pulses look similar – triangular and with a wide range of amplitudes. Here the pulse count is low, so the pulses in the high range were not recorded, because they are very rare. A trigger set very high would be needed to “catch” them with the oscilloscope.

1.2.1 Noise limitations

Noise is a major limiting factor in particle detection. It defines the minimum measurable particle energy and the minimum measurement resolution. It is hence important to minimise the electric noise in the detector signal. The major noise contribution comes from poor shielding from external electromagnetic sources. These often cause ringing, whereby the signal oscillates with a frequency defined by the external source. The ringing makes high-frequency measurements impossible. Another source of noise is the sensor itself. In the case of silicon, natural light increases the number of thermally excited free charge carriers, increasing the leakage current. This is not the case for diamond, which is with its high energy band gap insensitive to visible light. Nevertheless, any noise produced by the sensors is amplified by the signal amplifiers, which add an additional noise of the analogue electrical circuit to the amplified signal. Finally, the digitisers add the quantisation noise to the digitised signal. If

(9) there is no recombination!

The drift time is < 120 ps on the induced pulse width < 120 ps

⑧

Explaining the model for
the detector

⑨

Φ
fluence

⑦ how

→ be specific for diamonds!
→ energy level in
band gap → leakage

→ charge trapping → space
charge &
field
→ add references

1.3. RADIATION LIMITATIONS

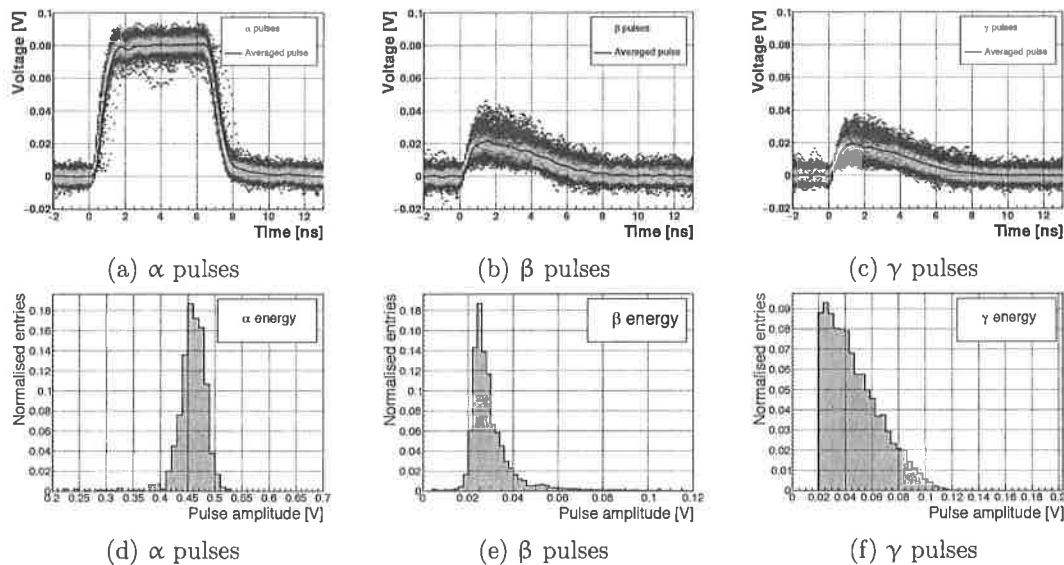


Figure 1.5: Superimposed and averaged pulses (a, b and c, current amplifier) and distributions of deposited energy (d, e, f, charge amplifier) for three types of radiation. Note the scale on the X axis of the distributions.

274 the measurement range is significantly higher than the actual measured signal, the
275 quantisation noise can be a significant contributor to the decrease of the overall mea-
276 surement resolution. → give the actual noise?

kernel noise, capacitive

277 1.3 Radiation limitation

⑦ etc as formulas!

278 Exposure to ionising radiation degrades sensors. It introduces charge traps by damag-
279 ing the sensor material. The electrons and holes created by the impinging particle get
280 trapped in these traps, decreasing the induced current on the electrodes. This yields
281 a lower integrated charge in an irradiated sensor than that in a non-irradiated one.
282 Charge collection efficiency is therefore correlated with the level of irradiation. This
283 section contains a study of the effects of pion ($\pi_{300 \text{ MeV}}$) irradiation on the charge
284 collection efficiency of sCVD diamond detectors. To carry out this study, two di-
285 amond samples were irradiated to $1 \times 10^{14} \pi \text{ cm}^{-2}$ (S79) and to $3.63 \times 10^{14} \pi \text{ cm}^{-2}$
286 (S52). Then a test beam campaign was carried out to observe the charge collection
287 efficiency at different bias voltage settings. The highest achieved efficiency values
288 were used to determine the effective drop in efficiency with respect to received ra-
289 diation dose. A model [] defined by a collaboration researching diamond behaviour
290 RD42 was applied to the measured values and a damage factor was extracted. The
291 next subsection contains measurements and results of a long-term stability study us-
292 ing α and β particles. In particular, the charge collection efficiency as a function of
293 time was measured during the measurements with β and α radiation. To investigate
294 this effect on the scale of charge carriers, the change of TCT pulses with time was

⑥ noise for charge quantity amplifier
not noise in input signal as well as
dependence on detector capacitance

see Spieles 1
lectures
expanded in chapter 2

⑨: how do you calculate DPA for your sample?

CHAPTER 1. EXPERIMENTAL RESULTS

DIAMOND IRRADIATION STUDY

295 observed. Finally, a procedure that improves the pulse shape and with it the charge
296 collection is proposed.

297 1.3.1 Quantifying radiation damage in diamonds

298 Radiation damage in semiconductors is not easy to understand and quantify. It varies
299 with the type of radiation (particles or photons) and its energy. There are several
300 models existing [?, ?, ?] that try to explain the impact of irradiation and to provide
301 hardness factors to compare the radiation damage between different particles. The
302 standard way is to convert the damage into *neutron equivalent*. Some models have
303 been extensively verified with simulations and with experiments. In these experiments
304 charge collection in sensors is measured before and after irradiation. This procedure
305 is repeated several times, with a measurement point taken after every irradiation.
306 When a set of measurements of charge collection is plotted against the radiation
307 dose received by a specific particle at a specific energy, a damage factor k_λ can be
308 extracted. Damage factors have to be measured across a range of energies and types
309 of radiation to properly quantify the damage in the sensors. They are then compared
310 against the simulations to verify that the experimental observations are in line with
311 the theory.

312 Radiation damage in silicon is well understood and explained. Silicon sensors
313 have a relatively low cost and are widespread. This makes irradiation studies with
314 high statistics feasible. Diamond, on the other hand, is an expensive material and
315 the technology is relatively new as compared to silicon. Therefore not many institu-
316 tutes are carrying out diamond irradiation studies. To join the efforts, the RD42
317 collaboration [] was formed. It gathers the experimental data from diamond irradia-
318 tion studies. Unlike with silicon, the experimental results so far show no significant
319 correlation with the NIEL (non-ionising energy loss) model [?], which correlates de-
320 tector efficiency with the *number of lattice displacements*. Therefore an alternative
321 model was proposed [?], correlating the diamond efficiency with *displacements per*
322 *atom* (DPA) in the bulk. Figure 1.6 shows the DPA model for a range of energies of
323 proton, pion and neutron irradiation in diamond. According to the figure, a 300 MeV
324 pion beam damages the diamond bulk twice as much as a 24 GeV proton beam. The
325 data points obtained by RD42 are also added to the figure. They have been nor-
326 malised to damage by 24 GeV protons. Finally, the data point measured in the scope
327 of this thesis has been added for comparison.

328 Irradiation with a π_{300} MeV beam

329 The samples were irradiated at the Paul Scherrer Institute (PSI) [] by means of a
330 beam of pions with an energy of 300 MeV (kinetic energy 191.31 MeV) and with
331 a flux of up to $1.5 \times 10^{14} \pi \text{ cm}^{-2}$ per day. The system has a 10 % uncertainty on
332 the beam energy. In addition, due to the uncertainty on the hardness factor, the
333 equivalent fluencies have an error of $\pm 20\%$. Looking at figure 1.6, π_{300} MeV sit on a
334 steep section of the DPA distribution. After fitting a linear function to this part of

⑩ What is "equivalent fluence"? Which part 2
why does it relate to hardness factor?

1.3. RADIATION LIMITATIONS

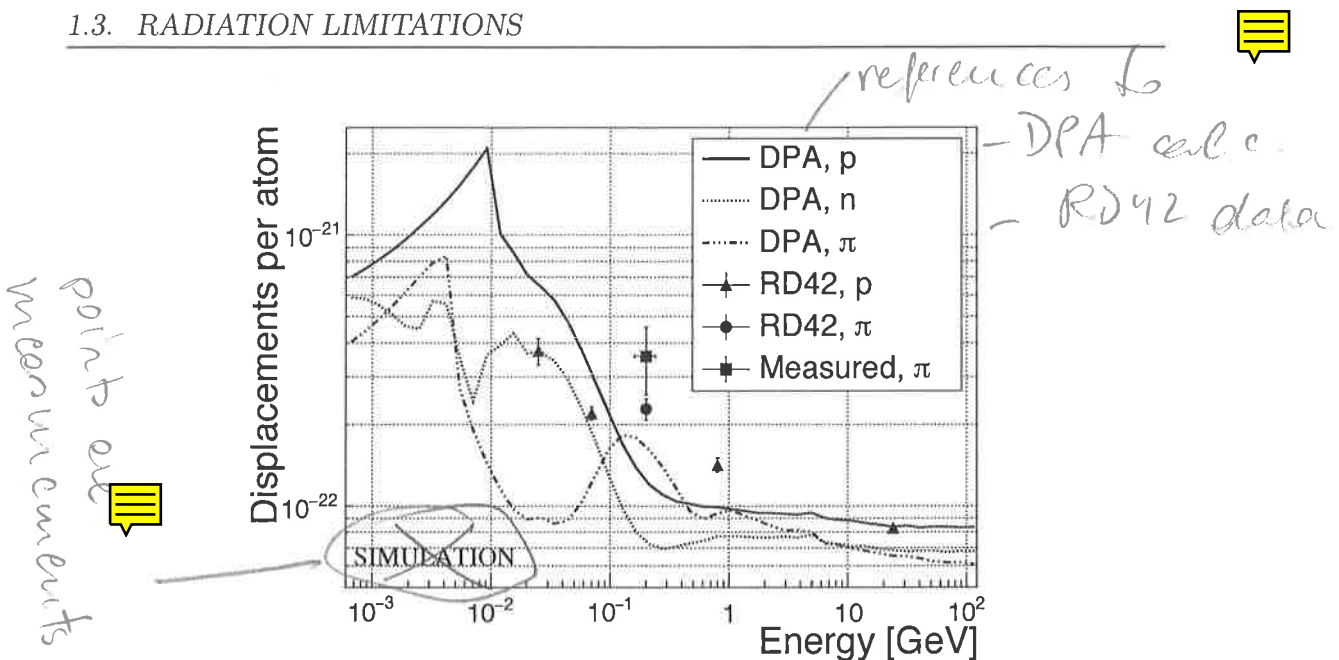


Figure 1.6: Diamond radiation damage - a model based on displacements per atom [1]. Added are data points for protons and pions by RD42 and one data point for pions measured in the scope of this thesis.

the distribution, the error on the DPA due to the uncertainty on the beam energy amounts to 7 %. Overall error on the fluency is therefore the root mean square of the uncertainty on the DPA and the uncertainty on the hardness factor: $\sigma = 21 \%$.

Two diamond samples, S52 and S79, were put in the π 300 MeV beam in the 2014 PSI irradiation campaign; S52 to $(1 \pm 0.21) \times 10^{14} \pi \text{ cm}^{-2}$ and S79 to $(3.63 \pm 0.77) \times 10^{14} \pi \text{ cm}^{-2}$. During the process, the golden electrodes got slightly activated, but the activation decreased in two weeks.

342 Charge collection efficiency and charge collection distance

Three diamonds – non-irradiated S37 and irradiated S52 and S79 – were tested in a $\pi_{120 \text{ GeV}}$ test beam [1] before and after irradiation. The goal was to estimate the charge collection efficiency (CCE) and charge collection distance (CCD) as a function of irradiation dose. The samples were primed (pumped) prior to data taking using a ^{90}Sr radioactive source. The data were then taken at a range of bias voltages ranging from 30 V to 900 V, yielding between $0.06 \text{ V}/\mu\text{m}$ and $1.8 \text{ V}/\mu\text{m}$ electrical field in the bulk. Every data point contained approximately 5×10^4 measured particles. The charge deposited by the particles was measured using a CIVIDEC Cx charge preamplifier. As expected, the integrated amplitude spectrum followed a landau distribution. Its most probable value (MPV) was used to calculate the most probable collected charge Q_i :

$$Q_i [e] = Q_i [fC] \cdot 6.241 \times 10^{18} = \frac{\text{MPV} [\text{mV}]}{A [\text{mV}/fC]} \cdot 6.241 \times 10^{18} \quad (1.1)$$

$$1 e^- = 1.6 \cdot 10^{-19} \text{ C} \quad 12$$

$$= 1.6 \cdot 10^{-4} \text{ fC} \Rightarrow$$

$$Q [e^-] = \frac{\text{MPV} [\text{mV}]}{A [\text{mV}/\text{fC}]} \cdot 1.6 \cdot 10^{-4}$$

- (11) For 1.7.b: at what field is the charge per charge point taken?
- (12) Why is $Q(S52) > Q(S79)$, if $\phi(S52) > \phi(S79)$?? are the points mixed up?

CHAPTER 1. EXPERIMENTAL RESULTS DIAMOND IRRADIATION STUDY

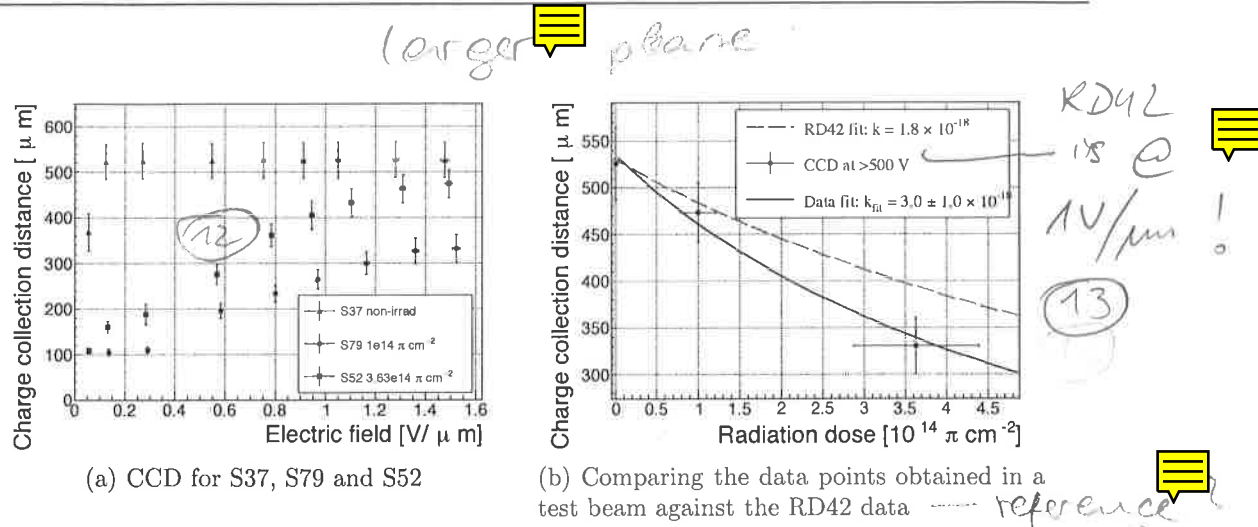


Figure 1.7: The charge collection distance at 500 V bias voltage for the three diamond samples was compared to the RD42 data for pion irradiation. The data points are about 5–15 % lower than expected from the RD42 data.

354 where $A = 9.2 \text{ mV/fC}$ is the preamplifier gain factor. The CCD was then calculated
 355 using the average number of electron-hole pairs produced per micrometer in diamond
 356 $\delta_d = 36 \text{ e-h } \mu\text{m}^{-1}$ (from table ??):

$$CCD = \frac{Q_i}{\delta d} \quad (1.2)$$

357 The resulting CCD for the three measured samples at bias voltages ranging from
 358 $0.2\text{--}1.6 \text{ V } \mu\text{m}^{-1}$ is shown in figure 1.7a. S37 exhibits full collection distance already
 359 at $0.4 \text{ V } \mu\text{m}^{-1}$ whereas the irradiated samples have a more gentle increase of CCD
 360 with increasing bias voltage. It is evident that at $1 \text{ V } \mu\text{m}^{-1}$ the maximum CCD has
 361 not been reached in the case of S79 and S52.

362 Irradiation damage factor

363 The irradiation damage factor k is a way to quantify irradiation damage of a specific
 364 particle at a specific energy. Via this factor different types of irradiation can be
 365 compared. It is obtained experimentally by measuring the CCD of a number of
 366 samples at various irradiation steps and fitting the equation 1.4 to the data. λ is the
 367 measured CCD, λ_0 is the CCD of a non-irradiated sample and Φ the radiation dose.

$$\frac{1}{\lambda} = \frac{1}{\lambda_0} + k_\lambda \cdot \Phi \quad (1.3)$$

$$\lambda = \frac{\lambda_0}{k_\lambda \lambda_0 \Phi + 1} \quad (1.4)$$

369 The data points with the maximum CCD obtained in the test beam measurements
 370 were plotted against radiation dose received (see figure 1.7b). Equation 1.4 was fitted
 371 to the data points and a damage factor $k_\lambda = (3.0 \pm 1.0) \times 10^{-18} \text{ } \mu\text{m}^{-1} \text{ cm}^{-2}$ was

(13) RD42 data are 2.2 per
 370 SC CVD! in pions, 4.8 is on pcVD

(15) time does not mean much without
alone rate give activity / dose rate

1.3. RADIATION LIMITATIONS

372 obtained. This value is for a factor of two higher than the damage factor obtained by
373 RD42. A possible cause is that the irradiated samples did not yet have a full charge
374 collection at $\text{V } \mu\text{m}^{-1}$. Also, with only two samples measured, the statistical
375 uncertainty was high. Nevertheless, it can be concluded that the 300 MeV pions
376 damage the diamond bulk more than the 24 GeV protons.

also true
for RD42

377 1.3.2 Long-term measurement stability

378 An important requirement for particle detectors is stable performance over long pe-
379 riods of time. For instance, the charge collection for a defined type and quantity of
380 radiation must not change over time or has to change in a predicted way. Diamonds
381 are stable as long as their environment and their operating point does not change
382 significantly. The stability of diamond detectors depends on many external factors.
383 The aim is to study the behaviour of diamond under controlled conditions, with the
384 goal to understand its limitations. One of these limitations is for sure the received
385 radiation dose. It might affect the long-term stability of the sensor during operation.

like...
? 

386 The three diamond samples (S37, S79 and S52) were exposed to two different types
387 of ionising radiation for a longer period to see if their behaviour changes over time.
388 Two parameters were observed in particular: 1) charge collection of β particles and
389 2) charge collection and ionisation profile of α particles. The results showed in both
390 cases that priming plays an important role in diamond measurement stability. The
391 β particles have a "healing" effect on the diamond; MIP detection is therefore rather
392 stable in the long run, despite the fact that the sensors had been degraded by means
393 of irradiation. Alpha particles, on the other hand, deteriorate the measurement,
394 probably by introducing space charge into the sensor bulk.

ref to later


What's
role
what is

a healing
effect?

what is
"rather"
stable

14

395 β long-term stability

396 The samples were intentionally not primed before the measurements took place. The
397 same initial conditions are usually found in HEP experiments. The measurement
398 setup consisted of a diamond sample with the Cx spectroscopic amplifier, a silicon
399 diode with a C6 amplifier for a trigger and a ^{90}Sr source on top. A particle emitted by
400 the source traversed the sensor bulk and hit the silicon diode, triggering the analogue
401 signal readout. The source was left on the top for the course of the experiment.
402 The measurements, however, took place at discrete times. For every data point,
403 approximately 10^4 triggers were recorded. The offline analysis of the recorded signal
404 pulse amplitudes yielded a landau distribution for every data point. The resulting
405 graph of charge collection over time (see figure 1.8) shows that the charge collection
406 efficiency improves over time when the diamond sensor is primed with a β source.
407 This is especially evident in the case of the two irradiated samples. S79 achieves close
408 to full efficiency whereas S52 reaches about 50 %. Both increases are significant.
409 After approximately 30 minutes the signal stabilises. As expected, the signal of the
410 non-irradiated S37 did not change with time – this pure sCVD diamond sample had
411 the maximum collection distance from the start.

15

(14) give stability as $\delta Q/Q$ vs time in percentage

CHAPTER 1. EXPERIMENTAL RESULTS
DIAMOND IRRADIATION STUDY

Consider how
replot as
 $Q(t)/Q(t=0)$

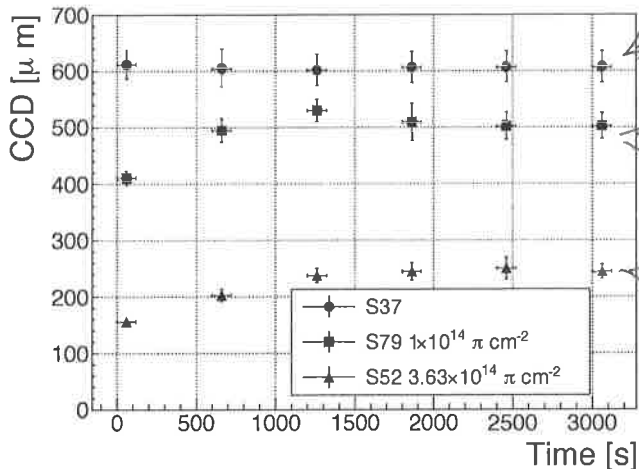


Figure 1.8: Increase of charge collection over time due to priming with the ^{90}Sr radioactive source

It should be noted that the ~~~2.28 MeV electrons~~ emitted by this source are not MIPs; their charge deposition is higher than that of an electron MIP, according to the Bethe-Bloch distribution [1]. Nevertheless, for the purpose of these measurements this energy was adequate since only the relative change in charge collection was of our interest.

To sum up, diamond is a good choice for β radiation detection. Even if damaged by radiation, it reaches a stable charge collection in the order of an hour. The efficiency decreases with received radiation dose, but the decrease can be accounted for if the damage factor and the rate energy of the particles are known. γ radiation has a similar impact on the diamond as the β . The impinging photons, if they interact with the diamond, prime the bulk, causing the increase in charge collection efficiency. The difference, however, is in the interaction probability (cross section), which is several orders of magnitude lower for gammas.

425 α long-term stability

This part discusses the stability of irradiated diamond sensors during α measurements. It is safe to assume that they will behave differently than when subject to β radiation. This is due to the point-like charge carrier creation when an α particle impinges the bulk. The energy is approximately 20 times higher than the most probable value of a MIP; deposited in a small volume, it will behave differently to the track-like energy deposition of MIPs. In addition, carriers of only one polarity drift through the sensor while the others almost instantly recombine with the adjacent electrode. Taking into account that the diamond bulk has been damaged by irradiation, these two phenomena might have an effect on the operation of the detector on a macro scale.

give exact difference: α energy loss of
 $241 \text{ keV} = Q = 5.98 \text{ eV}^{15} = 337 \text{ keV pairs}$

MIP @ 500 μm diamond = $\frac{240 \text{ keV}}{13.6 \text{ eV}} = 18 \text{ k pairs}$

(19) need to explain why efficiency drops! this is the most critical result from this measurement

1.3. RADIATION LIMITATIONS

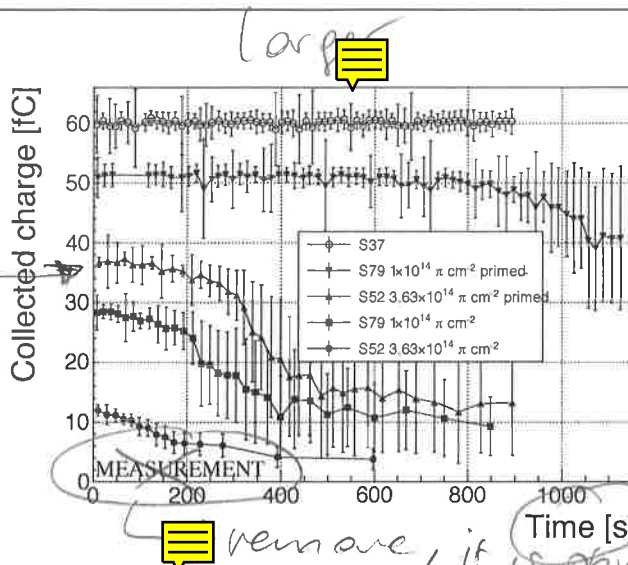


Figure 1.9: Comparison of collected charge with time for non-irradiated and irradiated diamond samples.

The measurement setup consisted of a PCB carrier for a diamond with a fitted ^{241}Am source and a vacuum chamber. The carrier was placed into the chamber, which was then evacuated. It acted as shielding for external noise pickup and ensured that the α particles didn't lose energy traveling through air. An SMA feedthrough ensured the electrical connection to the outside. The samples were measured before and after priming, at both polarities, to compare the behaviour of both electrons and holes as charge carriers. The scope of the measurements was to observe the changes in charge collection efficiency and/or in the pulse shapes.

The first test was carried out using the Cx spectroscopic amplifier. The bias voltage of the samples was set to +500 V and the signals from the diamond were measured for ~ 15 minutes. Figure 1.9 shows the results of these measurements. The collected charge for the non-irradiated sample was stable with time. It was expected that the irradiated samples will have a lower charge collection efficiency than the non-irradiated sample. However, their initial efficiency suddenly dropped after a certain period of time. The initial efficiency was improved after priming, but eventually deteriorated again. In addition, the spread of measured energies increased significantly. Also, the particle counting rate decreased with the decreased efficiency.

The next step was to observe the behaviour of the current pulse shapes with time using a C2 current amplifier. The shape of the pulse holds more information about the charge carrier properties in the sensor than solely the value of the integrated charge. This time only the primed S79 sample was tested. Both hole and electron collection were observed to determine whether they behave differently or not. The sample was measured long enough for the pulse shapes to start changing. The data in figures 1.10 show that the initially stable pulses start deteriorating – suddenly there are several different shapes, some still the same as at the beginning while the others with almost zero amplitude. These data are difficult to interpret. Nevertheless,

② the space charge region has to do with range of α , but not with one charge drifting → mention that space charge causes polarization field which contradicts applied field

CHAPTER 1. EXPERIMENTAL RESULTS DIAMOND IRRADIATION STUDY

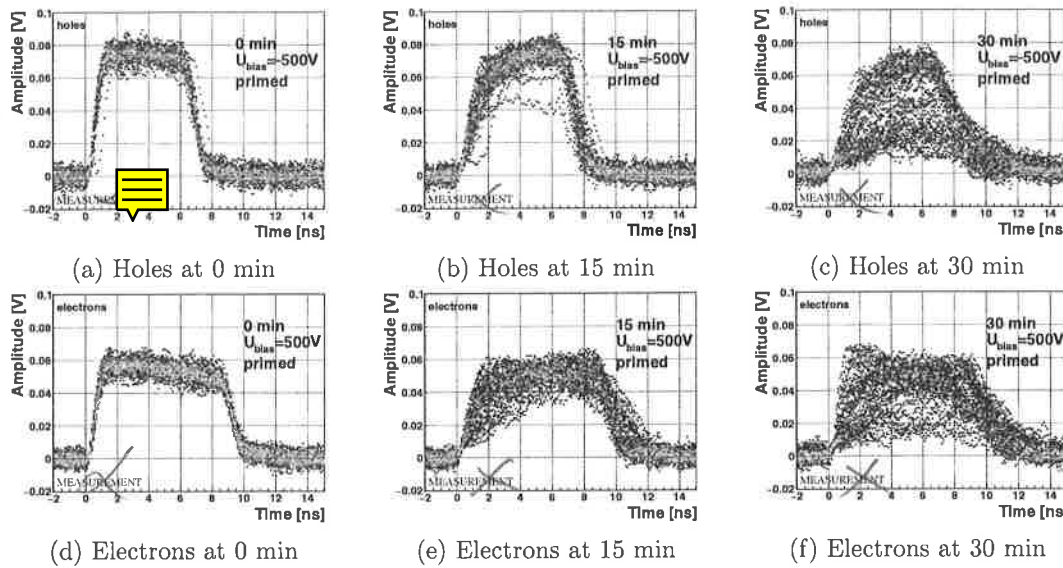


Figure 1.10: The signal of the irradiated and primed S79 deteriorates with time for both polarities. Every plot contains 60 superimposed pulses.

the idea is that some charges get trapped in the charge traps in the bulk for a long time, building up regions of space charge. Since only one charge flavour is drifting through the bulk whereas the other is quickly recombined, this already determines the imbalance in spatial distribution of trapped charges. The built up space charge affects the electric field, making it non-uniform. The non-uniform field in turn affects the drifting carriers, slowing them down or speeding them up, depending on the field gradient. Since the movement of the carriers is inducing the electric current, the field gradient can be observed in the signal. Unfortunately the effects are very convoluted, probably due to the entry point of the α particle.

At the beginning of every run, 60 reference pulses of the initial pulse were taken and plotted overlaid into a 2D histogram. An average pulse was extracted from this 2D distribution. Then a reference correlation between the reference pulses and the averaged pulse σ_{ref} was calculated. Subsequent data points also consisted of a set of 60 pulses. At every data point the correlation with the initial averaged pulse σ was calculated. From the ratio between the initial correlation σ_{ref} and discrete correlation values σ in time, the shape correlation $\text{Corr}_{\text{shape}}$ was calculated:

$$\text{Corr}_{\text{shape}}(t) = \frac{\sigma_{\text{ref}}}{\sigma} = \frac{\sum_x \sum_y w_{\text{ref}} \cdot (y_{\text{avg}} - y_{\text{ref}})^2}{\sum_x \sum_y w \cdot (y_{\text{avg}} - y)^2}, \quad (1.5)$$

where y_{avg} is the amplitude of the current averaged pulse at time x , y_{ref} is the amplitude of the initial averaged pulse at time x , y is the amplitude of the superimposed pulses in the 2D histogram and w and w_{ref} are weights for the superimposed pulses for the current data point and the initial data point.

Figure 1.11 shows the resulting time-resolved shape correlations. From the data obtained it can be concluded initial pulse shape quickly starts deteriorating. In fact,

② explain what $y_{\text{avg}}, y_{\text{ref}}$ and y depends on "t"

Comment on equation 1.5 :

- this is really a correlation function
- it is in essence a division of the error² on the mean of $y(x)$ by the variance of $y(x)$

1.3. RADIATION LIMITATIONS

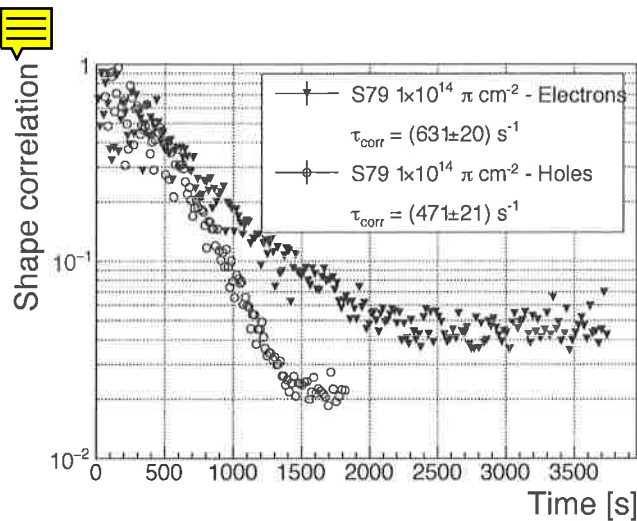


Figure 1.11: Deterioration of the pulse correlation with time

484 the deterioration of the shape correlation follows an exponential decay function, which
485 was fitted to the data. The resulting decay constants for electrons and holes are
486 $\tau_{\text{corr}_e} = (631 \pm 20) \text{ s}^{-1}$ and $\tau_{\text{corr}_h} = (471 \pm 21) \text{ s}^{-1}$. The electrons seem to retain the
487 initial shape for longer. The deteriorated shapes also seem to be for a factor of 2
488 better than those of the holes.

489 Finally, an effort has made to find a way for the pulse shapes to return to their
490 initial state. Five methods were tested:

- 491 1. Removing the source and leaving the bias voltage switched on,
- 492 2. Removing the source and switching the bias voltage off,
- 493 3. Priming with γ without bias voltage,
- 494 4. Priming with β with bias voltage switched on and
- 495 5. Priming with β without bias voltage.

496 The diamond sample S79 was first primed using a ⁹⁰Sr source for about one hour.
497 Then the bias voltage was switched on and an ²⁴¹Am source was put on top. The
498 pulses produced by the impinging α particles had a proper rectangular pulse at the
499 beginning, but then started changing in an erratic way, as described in the text above.
500 After approximately 30 minutes, one of the methods was tested. When a "healing"
501 procedure was started, a set of 60 pulses was taken at irregular points of time to
502 observe the change in the pulse shape and to assess the quality of the "healing"
503 procedure. Then the bias voltage was switched off and the sample was primed again
504 to reset its state before starting with the next run.

505 It turns out that the methods (3) and (5) improve the shape, method (2) helps
506 slowly, (1) does not show any change with time and (4) at first improves, but then
507 significantly degrades the shape. The effect observed in method (4) has already been

what is the
close for β & γ

(23) the space charge is neutralized how?

CHAPTER 1. EXPERIMENTAL RESULTS DIAMOND IRRADIATION STUDY

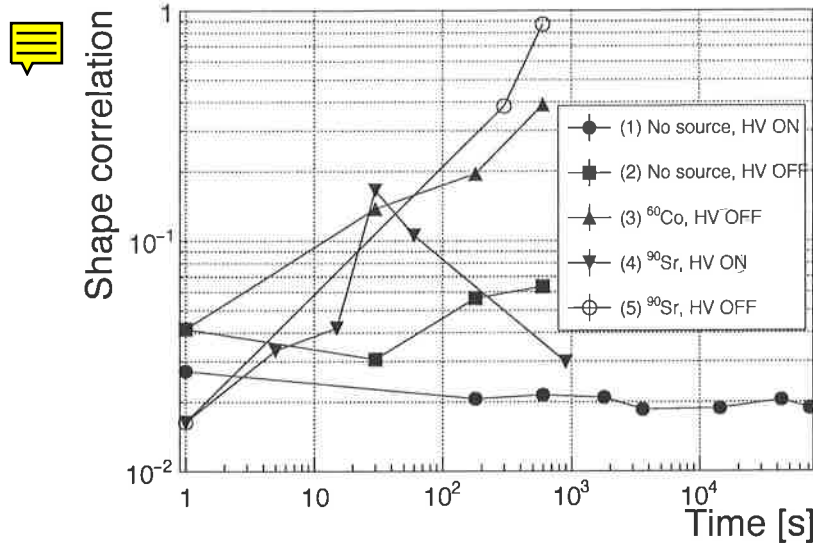


Figure 1.12: Five procedures of the “healing” process for an irradiated diamond that was exposed to α radiation at bias voltage switched on for at least 30 minutes.

described in [?]. The “healing” process therefore depends on the rate of radiation, the bias voltage and the time of exposure. The ionising radiation creates free charges, which quickly recombine close to the place of generation. It is likely that they also release the charges trapped during the measurement, reducing the overall effect of the space charge. The traps get filled with both flavours of carriers, thus they are neutralised. The pulse shape gradually returns to its initial state.

Procedure	Source	Bias voltage	Effectiveness
1	/	ON	no
2	/	/	slow
3	^{60}Co	/	YES
4	^{90}Sr	ON	no
5	^{90}Sr	/	YES

Table 1.2: Effectiveness of healing procedures

In summary, the shape of the pulses caused by α radiation changes with time for irradiated samples. The shape of the pulses gets distorted and becomes erratic. Charge collection decreases and its spread increases. This happens even faster for non-primed diamonds. To “heal” the diamond – to bring the pulse shapes back to their initial shape – the sample must be primed using a β or a γ source for several minutes at the bias voltage set to 0 V. Switching to the inverse polarity for a few seconds helps a bit, but in a long run distorts the signal, which cannot get back to its initial shape.

(24) : The exciton is the bound state
of e^- & h^+ , not the phonon

80 meV: Just say that the exciton binding energy
in 80 meV

1.4. TEMPERATURE LIMITATIONS

1.4 Temperature limitations

A test was carried out to evaluate the effect of temperature changes on the output signal of the diamond sensors. A cryostat filled with liquid helium was used to cool down the sensor during the measurement process. The current signal response to α -particles was measured at 18 temperature points between 4 K and 295 K. At every temperature point, a set of 300 pulses was read out at various bias voltages. Resulting data showed that the charge collection is stable down to 150 K, where it starts decreasing and stabilises again at about one third of the initial value at 75 K. This behaviour was first measured and discussed by H. Jansen [?].

The band gap energy in diamond is equal to $E_g = 5.5$ eV while the average energy to produce an electron-hole pair is $E_{e-h} = 13.25$ eV. This means there is excessive energy deposited in the diamond bulk. The impinging α -particle stops within $\sim 10 \mu\text{m}$ of the bulk, transferring all its energy to the lattice. A part of this energy, approximately 40 %, directly ionises the carbon atoms, creating free electron-hole pairs. The remaining energy, however, is converted into lattice vibrations (phonons [?]). This means that the lattice within the ionisation volume (approximately $\sim 10 \mu\text{m} \times \sim 2 \text{ nm}$ in size) is briefly heated up. The hot plasma then cools down to the temperature of the surrounding material by heat dissipation, (i.e. phonon transport).

The positively charged hole and negatively charged electron in the hole attract each other via the Coulomb force and may undergo a bonding process during which a phonon is emitted. That phonon is referred to as *exciton* [?]. The electron is pushed to a exciton energy band, which is 80 meV under the conduction band. At higher temperatures, the lattice provides enough energy to excite the electron from the exciton state back to the valence band (*exciton recombination* [?]). At lower temperatures, however, the exciton lifetime increases, which means that it will take a longer time for the electrons to get re-excited to the valence band. The re-excitation lifetime at room temperature is $\sim 30 \text{ ps}$, increasing to $\sim 150 \mu\text{s}$ at 50 K. [cold reference]

1.4.1 Temperature-variant α -TCT before irradiation

Three sCVD diamond samples were tested at a range of temperatures using the α -TCT technique. At each temperature point, the bias voltage was set to several positive and negative values. A set of 300 pulses was recorded at every data point and averaged offline. The resulting averaged pulses of sample S37 at the 260 K temperature point and a bias voltage of $\pm 400 \text{ V}$, $\pm 500 \text{ V}$ and $\pm 700 \text{ V}$ are shown in figure 1.13. The pulses induced by holes as charge carriers are shorter than those induced by electrons, which means that holes travel faster in diamond. The area of the pulse, however, is the same for both polarities, which corresponds to the fact that the same amount of charges is drifting in both cases.

Figure 1.14 shows pulses at a bias voltage set to $\pm 500 \text{ V}$ across the range of temperatures between 4 K and 295 K – room temperature (RT). Several conclusions can be drawn by observing their shape. First, the pulse shapes change with decreasing temperature. The pulse time gets shorter, hinting at the faster carrier drift velocity

(25) The explanation for ^{20}Q decrease in mindy in section 1.4, excitons are mentioned but how do they relate to mindy Q?

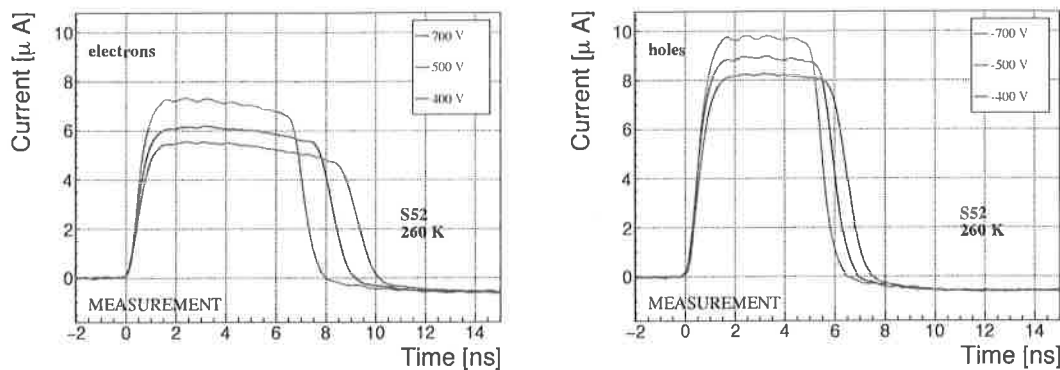


Figure 1.13: Varied bias voltage at a fixed temperature

*the
of
charge
trapping
likely due to
or could defect.*

565 v_{drift} . Second, between 150 K and 75 K there is a significant change in shape - the
566 time constant of the rising edge increases significantly and the pulse area decreases.
567 From 75 K down to 4 K there is no significant observable change. Last, the top of
568 the pulse at the S52 is not flat, which means that a portion of the drifting charge is
569 lost along its way. This could be due to impurities in the diamond bulk, which act
570 as charge traps, or due to the space charge built up in the bulk. A linear pulse top
571 hints on the latter. All-in-all, the pulse shape changes significantly with temperature,
572 which is predicted by Jansen's model.

573 1.4.2 Temperature-variant α -TCT after irradiation

574 The irradiated S79 and S52 were re-tested in the cryostat. The aim was to see how
575 their pulse shapes change with decreasing temperature, in particular the decaying
576 top of the pulses (see figure 1.15). The decay time gives information on trapping of
577 charge carriers while travelling through the diamond bulk. A variation of the decay
578 time constant as a function of temperature might help to reveal the type and depth of
579 the charge traps. To observe these effects or lack thereof, a number of requirements
580 had to be met. First, the diamond samples were intentionally not primed prior
581 to the experiment because priming would improve the pulse shapes and possibly
582 change the decay time constant of the signal. Second, keeping in mind that the pulse
583 shape of irradiated diamonds changes with time, the length of the measurement of an
584 individual data point had to be short – of the order of 30 seconds. Last, the sequence
585 of the bias voltage settings was important, the reason for which is explained below.

586 Unfortunately it was not possible to avoid temporal pulse changes. For instance,
587 one measurement point took approximately one minute. After the measurement, the
588 bias voltage polarity was swapped for a few seconds to bring the diamond back into its
589 initial state. But a few seconds with respect to a minute was not enough. Therefore,
590 when the bias voltage was set to the next value, there was still some residual effect
591 of the previous measurement. Similar to the effects of polarisation, this effect was
592 also decreasing the pulse height. This can be observed in figure 1.15, which shows



1.4. TEMPERATURE LIMITATIONS

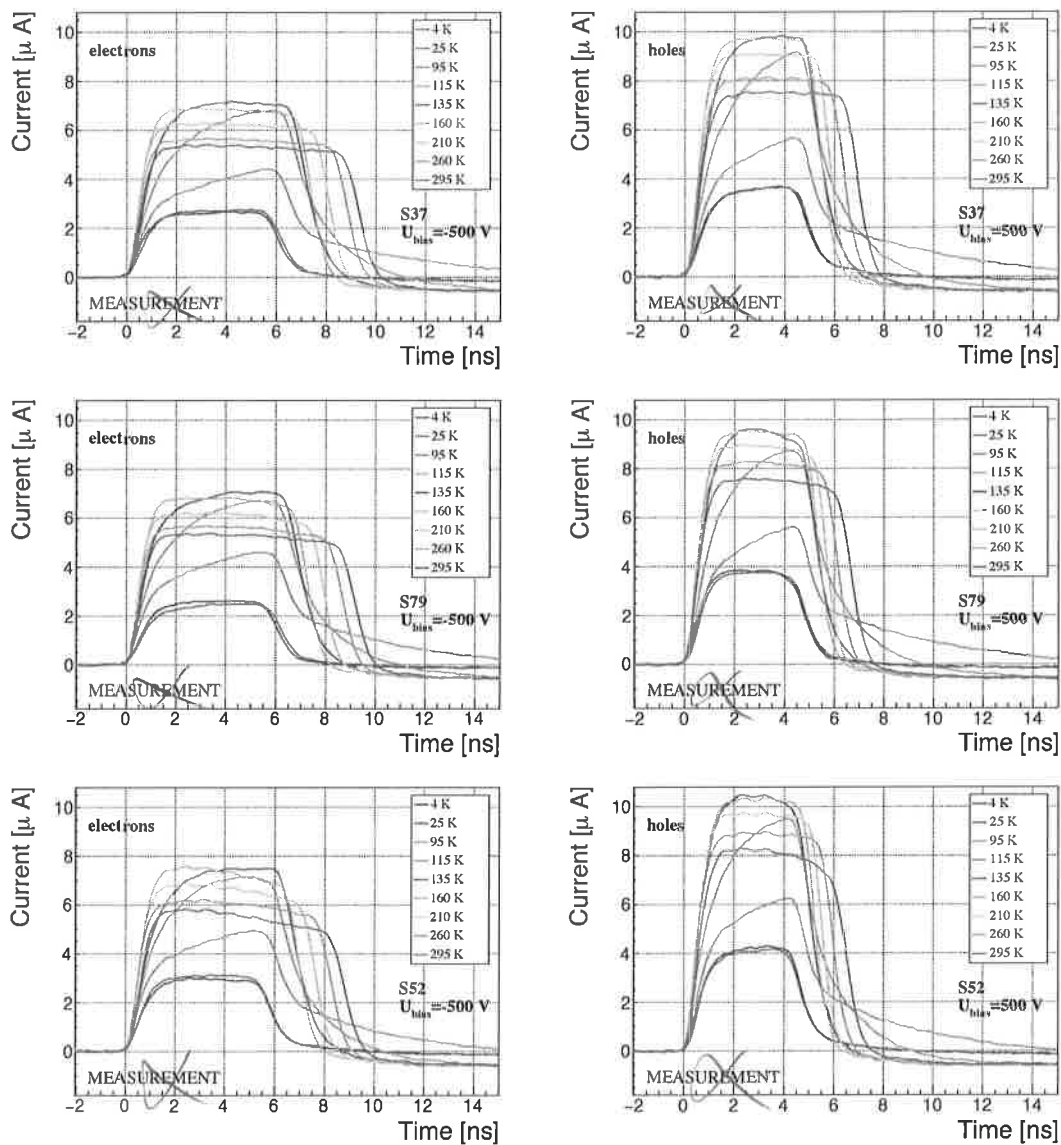


Figure 1.14: Several data points between 4 K and 295 K at a bias voltage of $\pm 500 \text{ V}$

CHAPTER 1. EXPERIMENTAL RESULTS DIAMOND IRRADIATION STUDY

the resulting pulses of S52 for bias voltages of ± 200 V, ± 300 V, ± 400 V and ± 500 V at 230 K and 260 K. In this case the measurements sequence was: 230 K (200 V, 300 V, 400 V, 500 V, -500 V, -400 V, -300 V), 260 K (-200 V, -300 V, -400 V, -500 V, 500 V, 400 V, 300 V). The changes in pulse shapes for holes at 230 K and 260 K cannot be attributed to the temperature change. Instead, the explanation could lie in diamond "polarisation". This means that, when exposed to an electric field with α measurements ongoing, the diamond builds up an internal electric field of inverse polarity, which effectively reduces the overall electric field. This internal field does not dissipate when the external bias voltage is switched off. It can be said that the diamond becomes "polarised". When switching the polarity of the external bias voltage, the internal and external electric field point in the same direction at the beginning, increasing the overall electric field and with it the pulse height. In figure 1.15, this happens when switching from 500 V to -500 V at 120 K. The built up polarisation contributes to the pulse having a sharp rising edge and a high amplitude. This effect decays during the next two voltage points. There would be a handful of ways to avoid this polarisation effect in the data:

1. After every data point invert the bias voltage and leave it to return to a neutral state for the same amount of time,
2. Make a hysteresis of data points, going from minimum negative to maximum positive bias several times,
3. Reduce the measurement time at every bias voltage setting.

Unfortunately, options (1) and (2) are very time consuming and would increase the overall experiment time to over one day. The third option would worsen the resulting averaged pulses. In the end an alternative option was chosen: alternating the starting bias voltage and the sequence at every temperature point. With this option, the highest possible systematic error in analysing the pulse shapes could be attained.

Figure 1.16 shows the irradiated S52 and S79 as well as the non-irradiated S37 for comparison, all at a bias voltage of ± 500 V and at several temperature points between 4 K and RT. It is evident that the radiation damage affected the shape of the pulses across all temperatures.

623 Collected charge as a function of temperature

The area below the current pulse is proportional to the charge collected by the diamond detector. The collected charge was observed as a function of temperature. First, the amplitude values of the averaged pulses at a bias voltage of ± 500 V and across the temperature range between 4 K and 295 K were integrated. Then a calibration factor was used to derive the charge for all data points. This factor was obtained using a Cx charge-sensitive amplifier. The resulting values for electrons and holes are plotted in figures 1.17a and 1.17b, respectively. This behaviour has already been observed and explained in []. The new contribution are the data points for the

1.4. TEMPERATURE LIMITATIONS

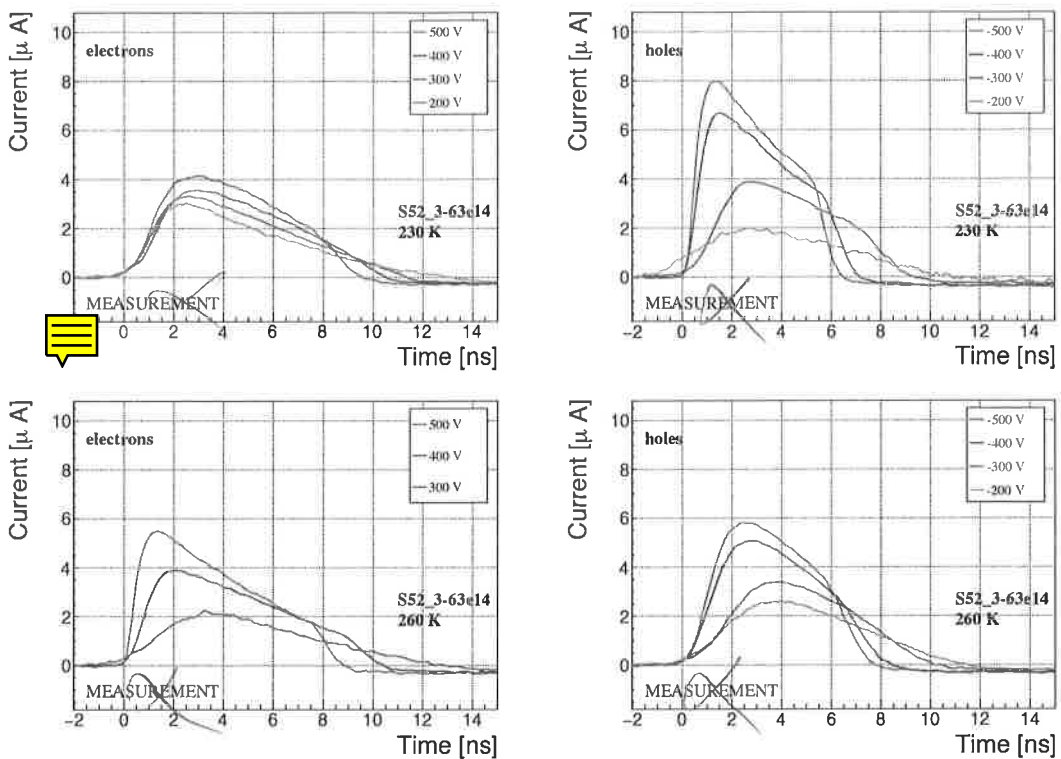


Figure 1.15: Varied bias voltage at a fixed temperature for an irradiated sample

632 irradiated samples. The values for them are lower than those of non-irradiated
633 samples, which is expected.

634 The values for all samples are fairly stable in the range between 4 K and 75 K
635 and between 150 K and 295 K. However, in the values for the irradiated S52 some
636 excursions can be observed. This is due to the sequence of the measurement steps,
637 which introduced a hysteresis effect and is explained in the preceding text.

638 The collected charge drops significantly from 150 K down to 75 K. In the non-
639 irradiated samples the values in the lower temperature range are approximately 0.30
640 of the values at the high range. For the irradiated ones this difference is lower – a
641 factor of 0.35 for S79 and 0.5 for S52. An interesting detail is that the ratio between
642 the values for non-irradiated samples and their irradiated counterparts at the lower
643 range is different than at the higher range. Looking at the values for the electron
644 collection in figure 1.17a: for S52 the lower ratio is equal to 1.28 and the higher equal
645 to 1.7. For S79 these ratios are 1.00 and 1.09, which means that the difference in charge
646 collection between 4 K and 75 K before and after irradiation is negligible.

647 Charge trapping

648 A decaying exponential function was fitted to the decaying top of the averaged pulses
649 at bias voltages of ± 400 V and ± 500 V across all temperatures excluding the tran-

CHAPTER 1. EXPERIMENTAL RESULTS
DIAMOND IRRADIATION STUDY

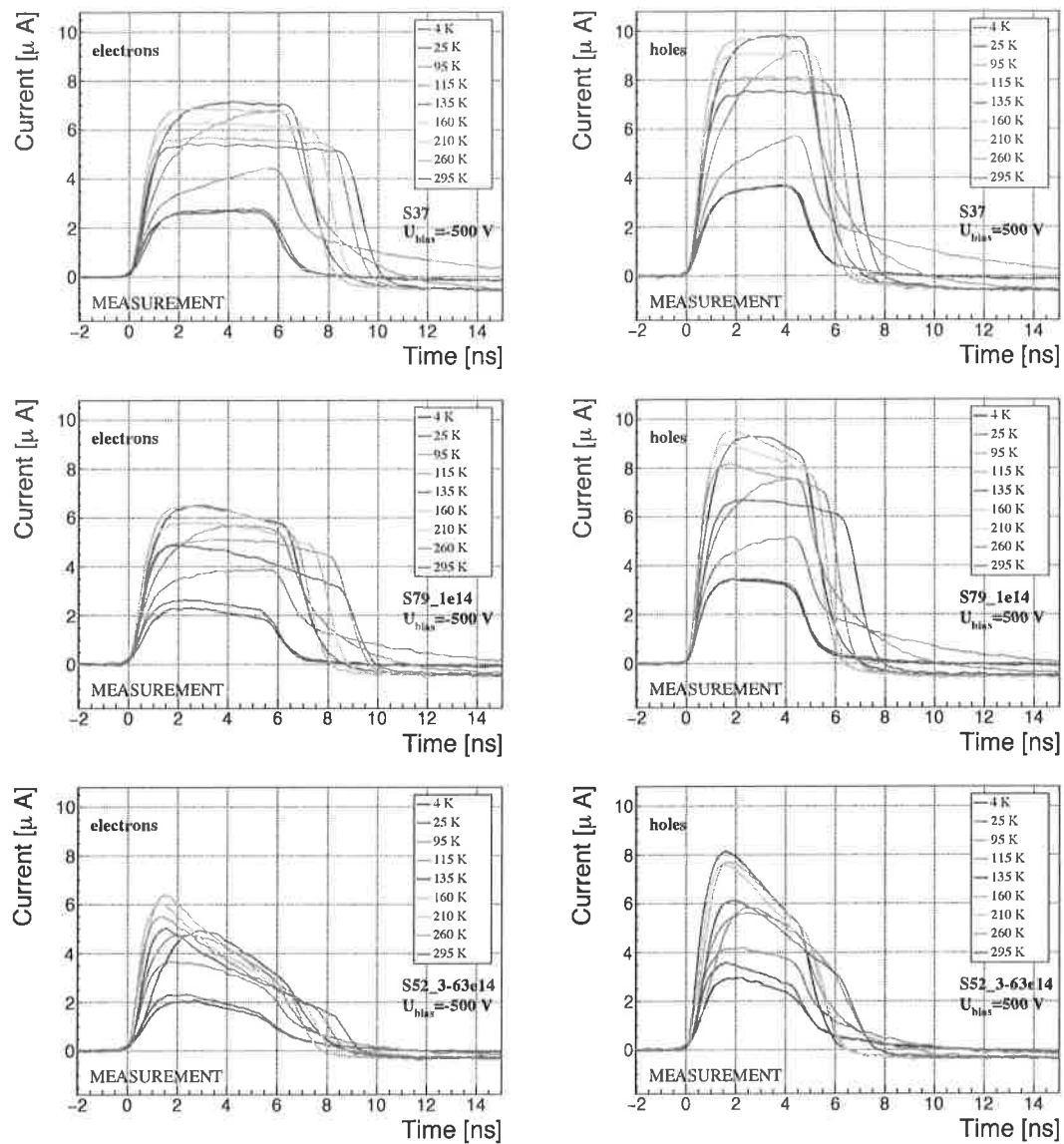


Figure 1.16: After irradiation: several data points between 4 K and 295 K at a bias voltage of ± 500 V

650 sitional range between 75 K and 150 K. The resulting decay time constants τ for
 651 an individual temperature point were not equal, which stems from the fact that the
 652 pulses changed with time due to "polarisation". This counts as a systematic error.
 653 Therefore all four fitted τ were averaged into one value representing the measurement
 654 at that temperature point. Figure 1.18a shows the fitted τ for the five samples be-
 655 tween 4 K and 295 K. In principle, the time constants should be infinite for a perfect
 656 and non-irradiated sample. Here a slightly tilted top of the pulse due to space charge
 657 was already successfully fitted with an exponential function, resulting in a τ of the
 658 order of 20 ns^{-1} . This is also why the spread is large. For the irradiated samples, the

not clear

E? (Voltage?) Unit? 25 is full 200 ns? what is the error on this?

(26) What is the interpretation of that in terms of charge traps and carrier energy level?

1.5. CONCLUSION

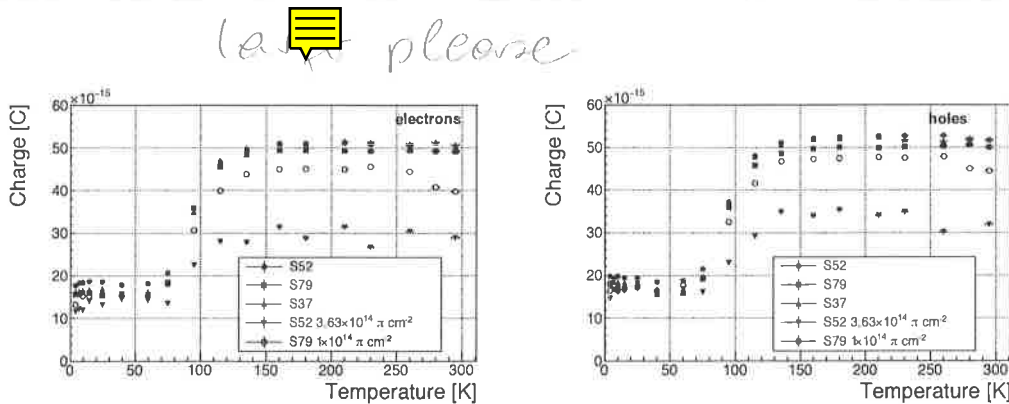


Figure 1.17: Collected charge as a function of temperature

fit becomes increasingly more meaningful. As seen in figure 1.18a, the fitted values of the irradiated samples are fairly stable across all temperatures. There is a slight increase in the decay time constant of the S52 from $(6.0 \pm 0.5) \text{ s}^{-1}$ above 150 K to $(8.5 \pm 0.9) \text{ s}^{-1}$ below 75 K. On the other hand, this step is not observable in the S79 data. With only one sample exhibiting this behaviour, the effect is not significant enough. Judging by the data acquired, the samples would need to be irradiated to doses above $1 \times 10^{14} \pi \text{ cm}^{-2}$ to quantify this effect in detail. So far this effect will not be regarded as significant for the scope of this thesis. Building on this assumption, the conclusion is that the signal decay time constant for irradiated sCVD diamond is constant across the temperature range between 4 K and 195 K, excluding the transitional range between 75 K and 150 K.

Taking into account the conclusions above, all the values can be averaged into one decay constant. Figure 1.18b shows these values for all samples as a function of the received $\pi_{300 \text{ MeV}}$ radiation dose. To estimate the carrier lifetime with respect to the radiation dose received, a similar model was used than that in section 1.5. This model states that the inverse of the carrier lifetime is linearly decreasing with increasing radiation dose:

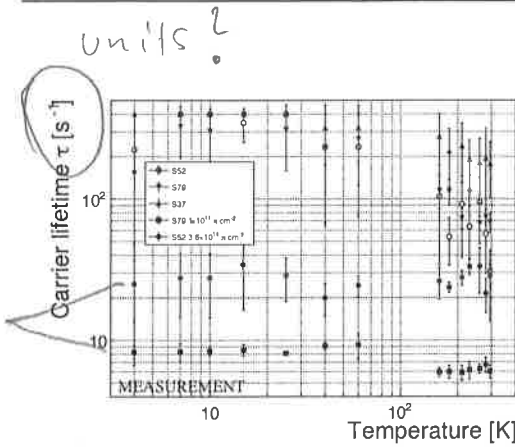
$$\frac{1}{\tau} = \frac{1}{\tau_0} + \kappa_\tau \cdot \Phi \quad (1.6)$$

$$\tau = \frac{\tau_0}{\kappa_\tau \tau_0 \Phi + 1} \quad (1.7)$$

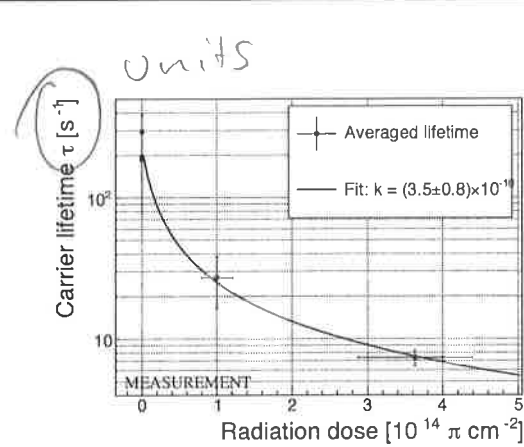
where τ_0 is the lifetime for a non-irradiated sample (real lifetime, therefore of the order of 400 s^{-1}), τ is the lifetime of an irradiated sample, Φ is the received radiation dose and κ_τ the lifetime degradation factor. For these data the fitted factor was equal to $\kappa_\tau = (3.6 \pm 0.8) \times 10^{-16} \text{ s cm}^2 \pi_{300 \text{ MeV}}^{-1}$. Using this factor, the steepness of the decay in the pulse shape with respect to radiation dose can be estimated. This can help when designing a system where current pulse shape is an important factor.

CHAPTER 1. EXPERIMENTAL RESULTS
DIAMOND IRRADIATION STUDY

units?
Carrier lifetime τ [s]
Temperature [K]
MEASUREMENT
Radiation dose $[10^{14} \pi \text{ cm}^{-2}]$



(a) Carrier lifetime as a function of temperature



(b) Carrier lifetime averaged over all temperatures as a function of π irradiation dose

Figure 1.18: Charge carrier lifetime decreases with irradiation, but is stable across the range of temperatures between 4 K – 75 K and 150 K – 295 K.

1.5 Conclusion

This chapter gives an overview of the capabilities and limitations of diamond as a particle detector. Three effects on diamond were studied – noise, radiation and temperature, the focus being on the latter two.

Two sCVD diamond detectors were irradiated with 300 MeV pions. They were tested alongside a non-irradiated sample to observe the changes in the ability to detect α , β and γ radiation. Their charge collection efficiency was measured in a test beam facility using . The results were compared to the results from the RD42 collaboration and a DPA model []. A radiation damage factor $k_\lambda = (3.0 \pm 1.0) \times 10^{-18} \mu\text{m}^{-1} \text{ cm}^{-2}$ was obtained for $\pi_{300 \text{ MeV}}$ particles. The data point was not in agreement with the data provided by RD42 nor with the model. However, the irradiation process and the low number of tested samples hold a relatively high statistical uncertainty. In addition, there was no diamond surface treatment done in between the measurements, as is the case in the study conducted by RD42. The results obtained in the course of these measurements will also be fed into the existing pool of data in the RD42 collaboration.

The next step was to test the long-term capabilities for α detection. The shape of the ionisation profile was investigated to determine the behaviour of the charge carriers in the irradiated diamond. An exponential decay was observed in the pulse, proving that there are charge traps in the bulk that were created during irradiation. Then a long-term stability test was carried out. The results show that the irradiated diamond detectors do not provide a stable and reliable long-term measurement of α particles. This might be due to a space-charge build-up in the bulk, which changes the electric field, affecting the charge carriers. A procedure to improve the pulse shape using β and γ radiation was proposed.

Finally, the diamond sensors were cooled down to temperatures between 4 K and

of irradiated
ionisation
profile

1.5. CONCLUSION

295 K. Their response to α particles was observed. The results of the non-irradiated and irradiated samples were compared. The effect of reduction for the number of drifting charges due to exciton recombination was observed in both sets of data. The second set had a superimposed effect of charge trapping during the drift, which was represented by an exponential decay in the signal. The decay time constant did not change with temperature. Therefore all temperature points for individual samples were averaged and the decay time constants were plotted against the received radiation dose. A damage factor equal to $\kappa_\tau = (3.6 \pm 0.8) \times 10^{-16} \text{ s cm}^2 \pi_{300 \text{ MeV}}^{-1}$ for non-primed diamonds was defined.